Quantum Phases and Chern-Simons Geometrics for the generation of a ligand targeting COVID-19-SARS-COV-2 SPIKE D614G binding sites.

1. Department of BiogenetoligandorolQMMIDDD/QPRPICA/MACHNOT/

QIICDNNDCA ADMET/QIICDNNDCA Stations, Biogenea Pharmaceuticals Ltd - Greece.

Grigoriadis Ioannis email: jgrigoriadis@biogenea.gr

Keywords: COVID19, SARS-COV-2 SPIKE D614G, Chern-Simons *Topological, AI-Quantum computing, Quantum-Inspired Evolutionary Algorithm Predictive toxicology, QSAR quantum gates,cheminfomratics artificial intelligence, phase data mining, machine learning, learning, cheminformatics*

Abstract

SARS coronavirus 2 (SARS-CoV-2) in the viral spike (S) encoding a SARS-COV-2 SPIKE D614G mutation protein predominate over time in locales revealing the dynamic aspects of its key viral processes where it is found, implying that this change enhances viral transmission. It has also been observed that retroviruses infected ACE2-expressing cells pseudotyped with SG614 that is presently affecting a growing number of countries markedly more efficiently than those with SD614. The availability of newer powerful computational resources, molecular modeling techniques, and cheminformatics quality data have made it feasible to generate reliable algebraic calculations to design new chemical entities, merging chemicals, recoring natural products, and a lot of other substances fuelling further development and growth of this AI-quantum based drug design field to balance the trade-off between the structural complexity and the quality of such biophysics predictions that cannot be obtained by any other method. In this paper, we strongly combine topology geometric methods targeting at the atomistic level the protein apparatus of the SARS-COV-2 virus that are simple in machine learning anti-viral characteristics, to propose computer-aided rational drug design strategies efficient in computing docking usage, and powerful enough to achieve very high accuracy levels for this in-silico effort for the generation of the AI-Quantum designed molecule the RoccustyrnaTM small molecule, a multi-targeting druggable scaffold (1S,2R,3S)−2−({[(1S,2S,4S,5R)−4−ethenyl−4−sulfonylbicyclo[3.2.0]heptan−2−yl]oxy}amino)−3−[(2R,5R)−5−(2−methyl−6−methylidene−6,9−dihydro−3H−purin−9−yl)−3−methylideneoxolan−2−yl]phosphirane−1−carbonitrile targeting the COVID-19-SARS-COV-2 SPIKE D614G mutation using Chern-Simons Topology Euclidean Geometric in a Lindenbaum-Tarski generated QSAR automating modeling and Artificial Intelligence-Driven Predictive Neural Networks.

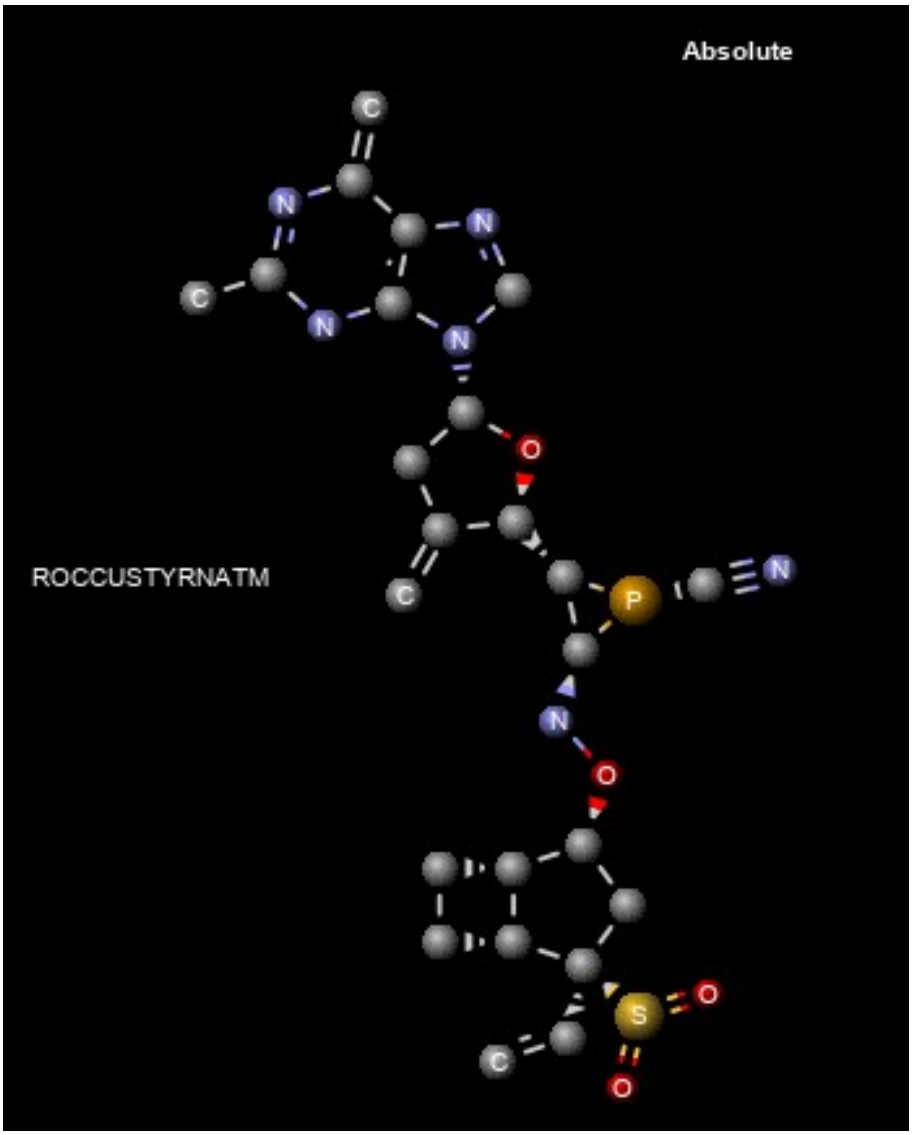

Introduction

(1,2,3)The COVID-19 disease which emerged in China at the end of 2019 was declared on March 2020 a pandemic by the World Health Organization (WHO) and is accountable for a large number of fatal cases. (2,4,5) On January 202, WHO committee declared a global health emergency (3,4-6) based on the rate of increasing spread of the infection (4,5-7) with a reproductive number (RN) in the range 2.0-6.5, 4 higher than SARS and MERS, (8) with more than 85,000 casualties and fatality rate of about 4%.(1-4) Collaborative efforts for Genomic characterization, (5,6,7-9) Evolution, phylogeny, high contagion rates, molecular epidemiology, of SARS coronavirus and epidemiology from scientists worldwide are underway to understand the rapid spread of the novel coronavirus (CoVs), and to develop effective interventions for control and prevention of the disease. (1-10) Coronaviruses are positive-single stranded, enveloped large RNA viruses that infect humans and a wide range of animals. (7,8-11) Tyrell and Bonne reported the first coronavirus in 1966, (11) who cultivated the viruses from the patients suffering with common cold. (4,6,7-10) In Latin, Corona means “crown” based on their shapes. As a megadiverse country, Brazil accounts for 10–20% of known living species in the world. However, a major part of the biological and chemical biodiversity in Brazil remains unexplored (17). (2–13,14,15,16,17) Molecular structure were

determined in heterodox interpretations (22) by solving the time-independent (21-22) Schrödinger equation: QM methods, vertex prizes and edge costs including ab initio Density Filed Theories (DFT) (23) and semi-empirical in place (24) of the quantum processor and energy among other observables,(25) under simulated sampling error as well as to reposition drugs about bonding may represent the similarities (26) and dissimilarities(27) between drugs and repurposed viral proteins respectively. (28) However, the Schrödinger equation cannot actually be solved for any but a one- data-driven (29) electron system methods (the hydrogen atom), (30) and approximations need to be made. According to QM, (2-19,23) an electron bound that converges quickly and reliably to an atom cannot possess any (2-17,21,22,23, 24,25,26,2728) arbitrary energy to produce the desired distribution by analyzing pharma-cological data or occupy any position in space using statistical and machine (23,24-37,38) learning concepts. The Lindenbaum-Tarski algebra logical spaces and vectorial re-presentations of the eigenvalue statements were used in this project and has been previously introduced as a 3D logical subspace allowing a well-defined position for each fragmented pharmacophore. This shows the application to quantum computing through the example of three coupled harmonic oscillators allows pure mechanical computation both for generating rules and inferences. (25,27,28) Since in previous studies It has been shown that Path selection for quantum repeater networks can be geometrically represented by Chern-Simons logical spaces and subspaces I decided to implement supersymmetric solutions and borel Singularities for N=2 allowing a quantum repeater based vectorial Supersymmetric Chern-Simons representation in this drug design project . (20,26,27,28-31) In general, the notions of Lindenbaum matrix and Lindenbaum-Tarski algebra have paved a way to further algebraization of logic, which had been begun by George Boole in the 19th century, as well as to a new branch of logic, model theory. Philosophical interpretations of QM were conditioned by ideals of what an explanatory theory should be. (Minkowski-type, wave-edge, etc), (20,27,32-33) as well as probabilistic transformations Algebraic multi-metrics (Triangle area, Bond-angle, etc) and the associated axiomatic formulations (AQFT) treat observables rather than states as foundational for the interaction information extraction. (20,33,34,35) In this project, we show an original strategy and an application to quantum computing through the example of two coupled harmonic black-hole oscillators obtained by molecular modeling and simulations as orthogonical coordinates applied for the design of a novel multi-chemo-structure against the crystal structure of COVID-19 protein targets in a Lindenbaum-Tarski generated QSAR automating modeling lead compound design approach. (29,35,36) A meta server and a Kappa-Symmetry C algebra of local observables were incorporated for the docking FDA approved small molecules, peptide-mimetic and humanized antibodies against potential targets of COVID-19 via a generalized procedure of Quantization of classical fields which were fused together with QSAR automating modeling to lead the commutation and anticommutation relations. (37,39,41,42) Dynamic niching and flexible heuristic genetic algorithmic states for automatic molecule recoring and fragmentation were applied to fragment and recore a database of 20,000+ molecules for use with the group contribution model Universal Quasichemical Functional Group Activity Coefficients (UNIFAC) against the structure and functions of SARS-CoV-2 as linear functional on the algebra of free energy docking observables. (37,38,40) Hybrid quantum repeater via a robust creation of entanglement between remote memory qubits were implemented for predicting drug targets and for multi-target and multi-site based virtual screening against COVID-19 (41,42) Flexible Topology Euclidean Geometric, were used to fragment molecules automatically in this molecular modeling and drug designing project on several parameters while keeping the definition of the groups as simple as possible. Artificial Intelligence-Driven Predictive Neural

Networks and Quantum- Inspired frameworks of parallel-Docking interactions were employed for supercritical entanglements introducing an advanced quantum mechanical inverse docking algorithm providing further insight to confirm the practicality of docking energy predictions for wild type and selected mutations for Nsp3 (papain-like, PLpro domain), Nsp5 Nsp15 (NendoU), (Mpro, 3CLpro), Nsp12 (RdRp), N protein and Spike in understanding the key element functions of SARS-CoV-2 protein pathways and in designing possible novel antiviral agents, from both an quantum algebraic and a cheminformatic perspective.

Materials and Methods

Preparation of the protein structures

The National Center (NCBI) database for Biotechnology Information was used to retrieve the S glycoprotein proteins of SARS-CoV-2. For the N protein, we aligned the clustered 31 conformations (1,2,35) from the 1731 full-length SARS-CoV-2 sequences and stored as a FASTA format file for analysis with Glu174 and Glu166 present in the opened RBD down conformation out of a total of 40 states COVID19 in the NMR-derived COVID19 associated protein structure (PDB codes, 6xs6,1xak,2g9t, 3fqq, 2ghv,6yb7) (1,3,4) to select a small subset representative of the protein flexibility downloaded from NCBI (30 April 202, txid2697049, NC_045512.2 with minimum length = 29,000 bp) as a coordinate reference and aligned using the MAFFT tool. (2-5,6) The BioEdit v7.2.3 sequence alignment editor was deployed to identify the conserved binding sites and short linear peptide region among the aligned sequences through multiple-sequence alignment (MSA) with ClustalW. The conserved alignment was visually generated, inspected and curated by preserving all nucleotides using Genbank NC_045512.2 as a coordinate reference in genomes such as the ball python genome, and further proceeded with the RSFIEDLLFNKV, e.g. KNFIDLLLAGF short linear motifs as identified between the Wuhan isolate beyond the limit of serious detection of the reptile shingle back for spike protein nidovirus 1 model construction by utilizing again the NC_045512.2 and annotated (ORFs) Open Reading Frames plus additional ORFs. We then provided to the DockThor-VS online docking platforms the protein structures in PDB format files of the SARS-CoV-2 (PDB codes, 6xs6,1xak,2g9t,3fqq,2ghv,6yb7) (1,3-10) as potential therapeutic drug targets (5-11,12) for the design of our new druggable scaffold named Roccustyrna. (13,14,15) For this main purpose, we initially selected the Nsp3, Nsp5 non-structural proteins (PLpro domain), Nsp15 (endoribonuclease), Nsp12 (RdRp) (5-16,17) and the structural proteins Spike and nucleocapsid protein (N protein). (9,10-21)) We then clustered the opened conformation states (31 alligned out of 40 conserved states) (9,17,22) using the Conformer Cluster web server tool (6,14,16) according to the position of the residues (5,7,8) Arg102, Glu166 and Tyr109 using the weighted sum of the centroid distances as the single linkage method. (7,8-12,22) Finally, the nearest to the pair group centroid structure per cluster was selected as the representative conformation of each group to be available at BiogenetoligandorolTM. In this article, we effectively use a AI-decision tree and an optimum quantum walk number of small chemical active chemical features from a collection of hundreds of them utilizing neural network and jointly docking free energy cumulative features and ranking method with input toxicity values taking both network decision tree parameters into account. In this work, we prepared the protein

structures using the Protein Preparation Wizard from the BiogenetoligandorolTM (BiogenetoligandorolTM, SynthocureTM, Thessaloniki, Biogenea Pharmaceuticals Ltd-GR, 2020). (8,13,17,22) hydrogen-bond optimization and Protonation assignment were applied by using the PROPKA and the ProtAssign publicly available software at the reported experimental pH (2-11,17) considering when available the presence of the bound small molecule (8-12,15,19).

Screening NuBEE Phyto-library and COVID2019 targets.

Virtual screening of the final proposed model and high throughput molecular docking based on existing literature were implemented to a collection of 9591 drugs including 2037 chemical structures of FDA-approved small molecule drugs and (2,3-14,17) over 6000 herbals and phytical extracts from the NuBBEDB updated database to get an insight into the potential inhibitors and to uncover chemical and biological druggable information from Brazilian biodiversity (4-6,17). Drugs selected for the docking studies with an ideal number of non-hydrogen and metal atoms not related with macromolecules, organic and inorganic active fragments (e.g., Pt, Fe, Hg, etc.) below 5 or above 10, phytical elements and drugs having Molecular Weight > 120, and already approved drugs that are consisted of original pharmacophoric elements of approved drugs into specific subcategories of prototropic tautomer, separate enantiomer, and protomer fingerprint alternatives. (7,8,17,18) Parallel Virtual screening technique for molecular docking was deployed at the center of the X: 228.75, Y: 190.82, and Z: 304.15. on its .pdbqt converted libraries of small molecules for the motif binding target sites using standard Web technologies such as CSS, HTML and JavaScript (AJAX) including graphics, text-based, and spectral files. (9,13-17) When more than one form of the screened drugs and phytical elements for the cross-validation (e.g., more than one protomer, more than one enantiomer, etc.) were screened, as suitable druggable candidates for recoring and fragmentating the forms with the highest GP and Docking Energy values were considered in the ranking. (14,16,17) Finally, drugs and selected NuBBEDB phytical extracts were docked according to the descending GP docking and binding energy values and only the screened hit candidates generating the highest binding energy values were considered for fragmenting and re-merging into the Roccustyrna small molecule using the BiogenetligandorolTM cluster of algorithms from the below. The whole set of molecules able to interact with the SARS-CoV PLpro enzyme were extracted after extensive machine learning similarity studies, retrieving only those small molecule ligands with absolute IC50 values. (2-17,34) This druggable .sdf set consisted of 11 PLpro approved inhibitors. Depending on the cross docking energy activities and fitness scoring analysis threshold', out of 11 compounds, 300 small molecule compounds with proven anti-viral properties were characterized as Actives and 153 molecules were categorized as Inactives. Physarum-prize-collective for molecular docking algorithm, Schrodinger-inspired Neural Matrix Factorization and a drug repositioning scoring analysis were implemented to a hybrid collection of the Natural Products of the Chemistry Institute of UNESP, Araraquara/SP and NuBBEDB phytical extracts (9-17,35) . (10-17,36) Protein-molecule complexes, (4,5,7,8-17) followed by structural relaxation were generated through (8,13-117) flexible-ligand rigid-receptor molecular docking (7,9,13,16-17) in these local energy minimization to optimize protein-ligand interactions capping the C- and N-terminal for each active druggable fragment with i-GEMDOCK (3-14,17) through cycles in all keeping conserved amino-acids within 4 Å of all the

docked ligands of each cation arrangement as considered for each relaxed chemical structure free of local energy and geometry minimizations. (1,2,5-17,34,35) Virtual screening experiments generated with KNIME pipelined DockThor Virtual Screening tool for the NuBBEDB and e-Drug3D dataset and for the ChEMBL database, at the reference pH (6.6 to 7.4) for all SARS-CoV-2 drug targets publicly available so far (e.g., N-terminal S1 subunit, PLpro, NendoU, (residue 14–685) in Spike Mpro,RdRp, and and a C-terminal S2 region N protein) using the wild isogenic type of the transcriptomic variants and 10 best matching phytical and chemical small molecule compounds (Table1a) were obtained as named, Colchicine, Raltegravir, Hexacosanol, Benzoxazolinon, Carboxy-Pentaric acid, Ursane, Antheraxanthin, RA-XIII, Crotonate and Byrsonima Coccolobifolia against the SARS-COV-2 protein targets of the (pdb:1xak), (pdb:6xs6) and (pdb:6lu7). (6,7-17,36) For each target, all crucial amino-acids involved virtually in this project of the cut-out parallel docking system when linked together with hydrogens were then collected, energetically favorable within 8 Å of any docked molecule onto the hydrophobic side chain and used to build a reduced phase docking system to be in contact with water where the “o C[C@]1(C[C@H] ([C@H]2 N1CN2)ONN1C[P@]1(C[C@H]1O[C@H](C[C” subscript in the first smiles term in the spaces of sequences refers to the difference of the free energy calculated using the protein-ligand (PL), protein (P) and ligand (L) sequenceof amino acid conformations bonded evaluations for dispersion/repulsion, hydrogen bonding, electrostatics, and desolvation to the central atom of each screened compound. (10,17,37) The GQM (X) refers to the energy of the cluster of the phytical small molecule known as the R group from the docked complex, in the free unbound state the fourth term corresponds to the change in conformational entropy, which were generated and the second and third unbound states of ligand side-chain conformations are calculated through local energy minimization as ΔGQMconf (X) = GQMo(X)− GQM (X) ,(X = L, P) (2) where GQMo (X) is the energy of the isolated active fragments in the conformation of the docked PL on both protein and molecule complex Inhibitors and conformations when applied Bioactivity-Guided Fractionations for the cluster of the selected compounds of the Colchicine, Raltegravir, Hexacosanol, Benzoxazolinon, Carboxy-Pentaric acid, Ursane, Antheraxanthin, RA-XIII, Crotonate and Byrsonima coccolobifolia Leaves and Stems to be fragmented, re-cored and accordingly merged into the RoccustyrnaTM small hyperactive druggable scaffold (3,4,17,36). The acknowledgement of the binding of the selected 8 phytical compounds to their full-genome evolutionary novel coronavirus (2019-nCoV) protein targets was accomplished using Molinspiration (http://www.molinspiration.com/cgi-bin/properties) and DrugBank (1,11,12,13,15,17,34).

Pharmacophoric-ODEs fragmentating, merging and recoring : Biogenetoligandorol AI-heuristic algorithm.

The patterns of this Biogenetoligandorol fragmentation scheme are sorted into the working inputs of the Galilean transformation by examining the “extended” Galilean transformation based on a set of heuristically determined descriptors moving with relative acceleration to a rigid system to a nonrotating geometric observer having an arbitrary time-dependent acceleration (20,21,27,28). (25,29) These descriptors as an applied nonconcurrent to both translate and rotatecan be, for example, the number of atoms describing the pattern of a force system which can both translate and rotate and be determined by the substitution as a polynomial in ip(r, t) = eiJ{r,t) (p(r', t). V'ip = (V'ip + iV 'f) eif, ρ¯sQFI≈∑i=01Re(ρi12)2

(1ρi11+1ρi22)+ (ρi11−ρi22)2ρi11+ρi22,ρ1ij=〈φi 〈1 ρs(0) φj〉 1〉ρ0ij=〈φi 〈0 ρs(0) φj〉 0〉 0〉 1〉H1=γB0·Sˆ1Re(ρi12)ρi12ρs(0)ρ¯s S〉=12(〉 − 01〉)30%ρs(0)ρ¯s=H⊗m 0V'2ip = {V'2ip + 2iV'f-V'(p+(pV'2f+ W ←S(I ⊗H)M1; <p(V'f)2)e‘f,i>= 〈Φ|MT(I3−NT) −2(ρ ⊗I2)|Φ〉 (f) + if<p) eif,and the Schrödinger equation becomes n 2 2 m (V,z(p + 2 iV'f-V'(p+ i(pV f - M = {M0,M1} (V 'fY <p)= ifi I3 ←E(m2); (*m2-dimensional identity*) ((<p + if(p) -g.(V '(p + i(pv' f)) where p+2 are the the number of bonds predicted or the number of double bonds. (20,25) The complete pharmacophoric fragmentation scheme was analyzed to compare similar series of chemical patterns that are contained in the chemical phase structures within the selected 10 hit compounds of the Colchicine, Raltegravir, Hexacosanol, Benzoxazolinon, Carboxy-Pentaric acid, Ursane, Antheraxanthin, RA-XIII, Crotonate and Byrsonima coccolobifolia. (20,35) Whenever searching for a specific pattern, if the group has such a parent pattern, the parent pattern is searched first eliminate the terms in V'(p,which gives f = — %-r'+ g(t). Then one can choose n g{t) such as to eliminate the purely time-dependent terms, and one finally arrives at, = (2mV '2(p + mf; ▪ r'(p = ih(p,ipir, t) =— ea h J (pir',t). (20,25,26) of the strong equivalence principle in quantum theory. After that, the child pharmacophoric pattern is searched in an inertial repeated merged system S asip = % (ml5 r, t) + ip2im2, r, t). (25,26,37) Then assume that one fragmented pharrmacophore can describe the same superposition in an accelerating to a larger ligand-receptor system S' that obeys (20), with § = £(r), £(0) = £(7) = , so that the system S' performs a closed quantum circuit and coincides with the chemical structure system the S at times t = 0 and t=T, such that r ’ iT) = r(7). (25-34,37) To avoid q { h q;}qreg q(3);creg c(3);reset q(0);reset q(1);reset q(2);h q(0);u2(pi/2,pi/2) q(1); incomplete (1Z)−2− {((2S,3S,5R)−5−(2−amino−6−oxo− 6,9−dihydro−3H−purin−9−yl)−3−hydroxyoxolan−2−yl) methylidene}−2−cyano− 1−({((2S,4R,5R)−2 group assignments, through two hydrogen-bonding interactions whenever a part into the S2 subsite of the structure relative to the complex between the cyano−1−({((2S,4R,5R)−2−methyl− 2− (methylamino)− 1,6−diazabicyclo with heptan−4−yl)oxy}imino)−1lambda5,2 lambda5−azaphosphiridin−1−ylium chemical groups of the cyclohexyl methyl is already recored and fragmented, the subsequent carbonyl oxygen matches have to be adjacent to the from the main-interacting chain amide of the residue Glu166 amino acid already occupied the space normally by the canonical S4- cyano−1−({((2S,4R,5R)−2−methyl−2−(methylamino)−1,6−diazabicyclo(3.2.0) heptan−4−yl) (1S,2R,3S)−2−({[(1S,2S,4S,5R)− 4−ethenyl−4−sulfonylbicyclo[3.2.0]heptan−2−yl]oxy}amino)−3−[(2R,5R)−5−(2−methyl−6−methylidene−6,9−dihydro−3H−purin−9−yl)−3−methylideneoxolan−2−yl]phosphirane−1−carbonitrile-oxy}imino)−1lambda5, 2lambda5−azaphosphiridin−1−ylium binding site of the PDB:6LU7 main protease. (26,31-39) As a first step, our Chern-Simons oriented fragmentation algorithm performs a quick fragmentation scheme search for extracting different chemical groups formed by the nucleophilic attack of the catalytic domains of the target proteases onto the α-carbon of my new Roccustyrna small molecule by applying the heuristic quantum phases for group prioritization when performing parent−child group prioritization as described above. (29,32-39) This topology geometric for pharmacophoric search and design indicating the canonical binding pockets moieties of a new small sized prototype that goes sequentially through a sorted fragmentation scheme, adding groups that are found in its active conformation phases and do not overlap with the cyano−1−({((2S,4R,5R)−2−methyl−2− (methylamino)−1,6− diazabicyclo(3.2.0)heptan−4−yl)

oxy}imino)− 1lambda5,2lambda5− azaphosphiridin−1−ylium chemical groups that were already screened. In case it successfully estimates a valid fragmentation, scheme this is taken as the phase solution relating to how one clustered pharmacophoric element occupies the space normally filled by the protease's substrate's interacting main chain; would describe the same phase in an alterantive XYZ coordinate smile system. (33,35-42) (13,14,15,16,17,19,23,26,27-38) This Lindenbaum-Tarski algebraic algorithm was implemented as a recursive algorithm that leads to enhancement of my novel small molecule's catalytic activity against the 3C protease−like domains I and II and performs a complete decision tree search of all possible combinations of fragmentation, merging and pharmacophoric recoring systems targeting in the in SARS-CoV Mpro. (12,13,17-21,27,28-39) To reduce the fragmentation space for the generation of salt-bridge interaction between the Glu290 and the new ligand that needs to be searched, the algorithm of the two independent Chern-Simons S=14π∫M3 A level k ∈ H4(BG, ℤ) ⟨A∧dA⟩k+ 13⟨A∧[A∧A]⟩ k(mod2π) actions with loop group at level k has that property 14π∫M3⟨A∧dA⟩k+1 3⟨A∧[A∧A]⟩ k(mod2π)[1]+sin$A$Vectk ($d\,A$+$A\wedge A$F)1 4π∫M3⟨A∧dA⟩k+13 ⟨A∧[A∧A]⟩ k(mod2π)[1]∧sin$A$Vectk($d\,A$+$A\wedge A$F) 14π∫M3⟨A∧dA⟩k+13 ⟨A∧[A∧A]⟩k (mod2π)[1]F= dA+A∧A Repk(dA+A∧A AGA) Repss(Fq$\mathfrak{g}$) [or Repk(AF$\mathfrak{g}$)] and Rep (Dk (ℂ[G]))=Repf($\mathcal{A}$G,k) equation (1) on the heuristic level of path integrals (AA is the potential 11-form and FF is the field strength 224-form) was applied where the partition function for the Chern-Simons theory when associated with knot theory is the modulus square of the partition function. (22,27,28,35) This In Silico approach keeps track of the solutions already found of the selected group of the selected hit candidates which were fragmented, recored and superposed in a non-relativistic quantum mechanics environment and finally led us to the complete Roccustyrna chemical structure. (20,28,29,30) If several chemical space solutions were found in the phase end, the combined theory has a sequence of similar such function spaces of finite but arbitrarily large selected dimension, where the partition dimension increases with the finite resolution of relative knot space measurements to the first dihydro−3H−purin−9−yl)− system when exctracted from the 10 hit selected small molecules as the possible chemical bimodules over a hyperfinite III1 factor solutions which were sorted by the number of different SARS-CoV Mpro, PDB entry 6lu7 receptor patterns. The Roccustyrna small molecule is the the fusion product of such chemical space representations of negative energy selected representations as merged into the connection form, ⟨ ⟩k:$\mathfrak{g}$ ⊗ $\mathfrak{g}$ → □ of the 6,9−dihydro−3H− purin loop group. This small molecule prototype was obtained directly from the solution of the LocG(S1) $CS_{G,k}(S_1) = Vect_{kG}[G] = Rep(D_k(C[G])) = Z(Vect_k[G])$ equation (2) by a procedure akin to geometric quantization as derived by a first phase solution was taken as the 13⟨A∧[A∧A]⟩ k(mod2π) equation (3) determined fragmentation. (36,37,39) and larger groups are prioritized over smaller chemical patterns with potential antiviral properties of the (1S,2R,3S)−2−({[(1S,2S,4S,5R)−4− ethenyl−4− sulfonylbicyclo[3.2.0] heptan−2−yl]oxy}amino)−3−[(2R,5R)−5− (2−methyl−6− methylidene−6,9−dihydro−3H−purin−9−yl)−3−methylideneoxolan−2−yl]phosphirane−1−carbonitrile patterns.

Roccustyrna ligand Protein targets

The docking engine employed in this computer-aided drug design effort is the DockThor program, which generates preparations of the acceptable topology files for the Roccustyrna ligand for the protein (.in) and ligand cofactors (.top) and a specific input .pdb file containing our prototype's ligand atoms and Roccustyrna partial charges from the MMFF94S49 force field. (19,21,37,42) The .pdbqt file of the Roccustyrna new ligand was generated by the MMFFLigand software, which is based on the utilities of the OpenBabel chemical toolbox for extracting atom types and partial charges with MMFF94S applied force field, and for the identification of the rotatable bonds, and calculating the properties necessary for computing the intramolecular interactions. (16,17,41) In the MMFFLigand, all hydrogen atoms were removed and the PdbThorBox software was utilized to set the protein atomic types, and the partial ionization charges from the MMFF94S force field analysis considering the nonpolar atomic groups as implicit to rebuild missing residue side chain atoms. (3-9,31) Thus, in this KNIME based GEMDOCK-DockThor-Virtual Screening platform, both the Roccustyrna small molecule, SARS-COV-2 protein targets, and cofactors were treated again with the MMFF94S force field by keeping the same set of equations and parameters that define the new molecule's molecular force field parameterizations. (2,31-40) The preparations of the steps to be used for diagonal force field for modeling such as modifying the protonation state of all the keeping amino acid residues, to parameterize a simple group of knots and atoms by adding metal complexes, hydrogen atoms and freezing rotatable bonds was done interactively for a variety of all-Roccustyrna atoms in the publically available web servers and performed automatically by the programs cited without the need for intervention. (3,15,16,17) The search docking space to rapidly simulate the Roccustyrna's molecular systems and the configuration of the new molecule's grid box were interactively set in the KNIME designed BiogenetoligandorolTM pipeline which were represented as a grid box and the docking potentials are stored at the best grid points for the description of the Roccustyrna's molecular energetic and structures through the parameters of the center of coordinates, size of the grid and discretization (i.e., the spacing between the grid points). (5,13,29,31) The initial population for the rotational, and translational, was randomly generated within the conformational degrees and grid box using random values of freedom of the Roccustyrna ligand. (15,16,17, 38) For each SARS-CoV-2 therapeutic target DockThor-VS default parameters were uploaded as a recommended set of parameters for the grid box (i.e., center and grid sizes) which can be used or modified according to the objectives of this docking experiment which was specially designed to deal with highly flexible ligands such as the Roccustyrna small molecule. (15-29,31) In this strategy, a replacement ligand based method was introduced by using a low mass phase phenotypic steady-state and crowding-based protocol and a multiple genetic parental algorithm as a Dynamic Solution Modified Restricted Tournament Selection (DSMRTS) approach, which provided us a better machine learning exploration of the energetic hypersurface for the identification of multiple quantum phase minima solutions in a single Hadamard run, preserving the population diversity of the generated structures. The default parameters of this parallel docking algorithm (named BiogenetoligandorolTM) is set in the KNIME-web server as follows: (i) 24 inverse docking runs, (ii) 1.000.000 evaluations per parallel docking run, (iii) population of the Roccustyrna individuals, (iv) maximum of 20 cluster small molecule top leaders on each parallel inverse docking run. For this sequential screening experiment, we also provided an alternative dataset of geometric parameters to improve the Euclidean space between the Roccustyrna

and protein interacting chains without significantly losing binding site accuracy (named EuTHTS Euclidean Topology Virtual Screening): (i) 120 docking runs, (ii) 200.000 evaluations per docking run, (iii) population of Roccustyrna individuals, (iv) maximum of 20 cluster leaders on each docking run. The docking experiments were performed on DockThor CPU nodes of the SDumont supercomputer, each one containing two processors Intel Xeon E5-2695v2 Ivy Bridge (12c @2,4 GHz) and 64 Gb of RAM memory. We validated the docking experiments through the redocking of the non-covalent Roccustyrna ligand present in the complexes 6W63 (Mpro) using the standard configuration, successfully predicting the co-crystallized conformation of each complex. In the crystallographic structure, this moiety is exposed to the solvent and has insufficient electronic density data. The free energy scoring function applied to score the best docked poses of the same Roccustyrna ligand was based on the sum of the following terms from the MMFF94S force field and is named "Total Energy (Etotal)": (i) intermolecular interaction energy calculated as the sum of the van der Waals between the hydroxyl and cyno groups (buffering constant δ = 0.35) and electrostatic potentials between the protein-ligand atom pairs, (ii) intramolecular interaction energy of the van der Waals and electrostatic potentials calculated as the sum between the 1-4 atom pairs, and (iii) torsional term of the ligand. All best docking poses generated during all the docking steps in this project were then low mass weight categorized and clustered by our in-house tool BiogenetoligandorolTM. The top docking energy-poses of each Roccustyrna-Protein complex were selected as top hit representatives of cluster energetic representatives to be made available in the homogenicity results analysis and Chern-Simons pharmacophoric fragmentation section (27,28). The binding affinity prediction and total energy ranking with the linear protein model and untailored for specific ligand interacted protein classes,of the Roccustyrna small molecule was generated by utilizing the DockTScoreGenLscoring function as a set of empirical scoring functions. Biogenetoligandorol cluster of DockTScore, PLIP, DockThor and GEMDOCK-AUTODOCK-VINA current docking scoring functions for protein and small molecule preparation take into account important terms, multiple protein-ligand binding, such as intermolecular interactions, binding affinity predictions, Roccustyrna's ligand entropy and desolvation of the specific target classes such as SARS-COV-2 6W63 (Mpro) proteases using protein-protein interactions (PPIs) trained with PdbThorBox and MMFFLigand sophisticated machine-learning derived topology algorithms totalizing 66 892 contacts between a carbon and a halogen, carbon or sulfur atom. The docking visualization of the SARS-COV-2 protein, cofactors and the Roccustyrna compound, the grid space location superposed with the protein targets of the (PDB codes of the PDB:6xs6,1xak,2g9t,3fqq, 2ghv,6yb7) (1-11,14-29,34, 35,36,39) and the docking outputs were generated with NGL, a WebGL-based library for intra-molecular visualization.

In silico Bioactivity Prediction and ADMET Analysis of the Roccustyrna small molecule.

The drug likeliness and bioactivity of the Roccustyrna small molecule were initially analyzed utilizing the Molinspiration server (http://www.molinspiration.com). (30,31) By using the Molinspiration web-tool, a cheminformatics multi-tasking software we calculated the Roccustyrna's molecular modeling docking energy properties as well as drug likeness and bioactivity prediction of our prototype ligand (Mabkhot et al., 2016). (40,41) In this section, the Molinspiration-based drug-likeness analysis web platform was incorporated to predict

the Roccustyrna's two important factors, including the polar surface area (PSA), and lipophilicity level (log P) directly associated with the pharmacokinetic properties (PK) of the same lead structure (Beetge et al., 2000). (31,40) Then, by uploading the Roccustyrna's smiles in the Molinspiration-based bioactivity analysis web server, we calculated the bioactivity score of this ligand through the systemic examinationion channel modulators, GPCR ligands, nuclear receptor ligands, kinase inhibitors, protease inhibitors, and other enzyme targets which were analyzed by sophisticated Bayesian statistics (Mabkhot et al., 2016). (5,7,40) The PK properties, such as adverse effect predictive modeling, Absorption, Distribution, Metabolism, Excretion, and Toxicity (ADMET), of the Roccustyrna pharmacophoric scaffold were predicted by utilizing the admerSAR v2.0 server (http://lmmd.ecust.edu.cn/admetsar2/) for the prediction of our novel Roccustyrna's ADMET properties on factors such as membrane permeability [designated by colon cancer cell line (Caco-2)], human intestinal absorption (HIA), and the status of either P-glycoprotein substrate or inhibitor. Finally, knowledge of these processes and more specifically the ability of the Roccustyrna's small molecule to penetrate the blood-brain barrier and its metabolism is of crucial importance to evaluate the risk of exposure to toxins and was evaluated by the MATE1, CYP, and OATP1B3 -OATP1B1testing models. The Excretion of the Roccustyrna ligand was estimated by applying the advanced matched molecular pair analysis (MMPA), based on the renal OCT substrate and the toxicity which was then predicted accordingly on the Human Ether-a-go-go-related gene inhibition, mutagenic status, carcinogenic status, and acute oral toxicity default parameters (30,31,40,41).

Results

In silico Prediction of the Roccustyrna ADMET Properties and Bioactivity Score

To predict important molecular properties such as logP, polar surface area, drug-likeness and bioactivity of our new prototype and small sized Roccustyrna ligand (1S,2R,3S)− 2−({[(1S,2S,4S,5R)−4− ethenyl−4−sulfonylbicyclo(1S,2R,3S)−2−({[(1S,2S, 4S,5R)−4− ethenyl−4−sulfonylbicyclo[3.2.0]heptan−2−yl]oxy}amino)−3−[(2R,5R)−5−(2−methyl−6−methylidene−6,9−dihydro−3H−purin−9−yl)−3−methylideneoxolan−2−yl]phosphirane−1−carbonitrile[3.2.0]heptan−2−yl]oxy}amino)−3−[(2R,5R)−5−(2−methyl−6−methylidene−6,9−dihydro−3H−purin−9−yl)−3−methylideneoxolan−2−yl]phosphirane−1−carbonitrile, the Molinspiration tool was employed as customized on the basis of this rational anti-viral drug design study.The milogP (Octanol-water partition coefficient logP) and TPSA (Topological polar surface area) values were calculated by utilizing the same online tool using Bayesian statistics. These In-Silico results indicated that the milogP value of the Roccustyrna small molecule was predicted as having optimum lipophilicity properties (logP < 5) (Han et al., 2019) in the aspect of dermal absorption and parallel artificial permeation (Table1c).

Screening of the Roccustyrna Inhibitor for Spike Protein-RBD-ACE2 Interaction

In this study we have shown that the QMMM designed Roccustyrna small molecule which was designed in silico by using Topology Euclidean Geometric and Artificial Intelligence-Driven Predictive Neural Networks was engaged in the binding domains of the protein targets of the (pdb:1xak) (Figure4a) with the docking energy values of the (T.Energy, I.Energy, vdW, Coul, NumRotors, RMSD, Score), (-19.625, -35.483, 7.633, -43.116, 7, -

5.813)Kcal/mol, (Tables1a,1b, 2a) The Roccustyrna chemical structure interacted into the binding sites of the protein targets (pdb:6w9c), (Figure4b),(Figure7e) with the negative docking energies of the (T.Energy, I.Energy, vdW, Coul, NumRotors, RMSD, Score), (-36.678 ,-55.648, -7.519, -48.129, 7, -6.762) Kcal/Mol. It also generated hydrophobic interactions when docked onto the binding cavities of the amino acid of the 168 PRO, A1, 02J C with the docking energy values of the 3.53, 2369, 1303, -10.425, 3.42, 72.447, -13.394, 3.19, 70.551Kcal/mol . Our new QMMM designed small molecule named Roccustyrna involved in the generation of the hydrogen bonding within the PJE:C:5 (PJE-010) 010:C:6 Interacting chain(s) while generating hydrophobic interactions when docked into the binding domains of the amino acid of the 25THR, A6, 010 C domains with the docking energy values of the 3.73, 2415, 179, -7.156, 21.406, 66.898 -8.709, 22.779, 70.002 Kcal/mol. (Figures1a,1b, 4,5a,5b,5c, 5d,6a,6b,6c,6d,6e,7a,7b) The Roccustyrna's active pharmacophoric site of the (methylamino)−1,6− diazabicyclo(3.2.0)heptan−4−yl)oxy}imino) interacted into the binding cavities of the amino acid of the 26 THR, A6 010C with the docking energy values of the 3.81, 2415, 186, -7.156, 21.406, 66.898, -6.155, 24.392, 64.757 Kcal/mol. The Roccustyrna's active pharmacophoric site of the dihydro−3H−purin−9−yl)−3− hydroxyoxolan generated an inhibitory effect which was involved in the generation of hydrogen bonds when docked into the binding cavities of the amino acid of the 143 GLY A 6 010 C with the docking energy values of the 1.93, 2.8, 145.29, 1105, 2411, -8.911, 17.849, 65.703 -8.918, 17.918, 62.905 Kcal/mol. The same prototype pharmacophoric elements named Roccustyrna when docked into the binding sites of the amino acid of the 164HIS, A5, PJE C2.generated hydrogen interactions with the binding energy values of the 16 3.07, 153.73, 2408, in the coupled atoms of the N3 and O2 with the docking energy values of the -12.282, 14.994, 67.123 -15.161, 15.336, 68.144 Kcal.Mol (Figures1a,1b,4,5a,5b, 5c,5d,6a,6b,6c,6d,6e). The binding patterns of the 02J:C:1 (02J) active sites of the amino acid 168 PRO, A1, 02J C binding domains generated hydrophobic interactions with docking energy values of the 3.53, 2369, 1303, -10.425, 3.42, 72.447, -13.394, 3.19, 70.551 inside the PJE:C:5 (PJE-010) + 010:C:6 interacting chain(s): A C of the amino acid of the 164HIS, A5, PJE C2. The Roccustyrna's pharmacophoric active site of the 2-lambda5−azaphosphiridin−1−ylium was engaged in hydrogen bonding interactions with the formation of hydrogen bonds inside the binding cavities of the amino acid of the 143 GLY, A6, 010 C with the docking energy values of the 1.93 2.80 145.29 1105, 3.81 2415 186 -7.156, 21.406, 66.898 -6.155, 24.392, 64.757 2411 O3 -8.911, 17.849, 65.703 -8.918, 17.918, 62.905, 2.16 3.07 153.73 2408 N3 1266 O2 -12.282, 14.994, 67.123 -15.161, 15.336, 68.144 Kcal/mol (Figures1a,1b,4,5a,5b, 5c,5d,6a,6b ,6c,6d,6e). The Roccustyrna small molecule involved also in the generation of the hydrophobic interactions within the binding domains of the amino acid of the 25 THR A 6 010 C with the docking energy values of the 3.73, 2415, 179, -7.156, 21.406, 66.898 -8.709, 22.779, 70.002Kcal/mol as illustrated in the (Figures1a,1b,2a, 2b,2c,2d,3a, 3b,3c,4a,4b, 5a,5b,5c,5d,6a,6b,6c,6d,6e). In this project, we implemented Quantum Heuristic Fragmentation Algorithms for the merging and recoring of the hit selected Drug Pair interactions by using Quantum Hamiltonians for the =γB·(Sˆ1+Sˆ2)+Iˆ·A·Sˆ2, Sˆi=(σx,σy,σz)Iˆρs(t)=TrI(U(t)ρ (0)U†(t)),ρI(0)=I/2P(t′)=dΔM(t′) ΔM=f(t′)dt′,ρ¯s=∫ −∞0f(t′)ρs(t′)dt′=∫0∞f(t)ρs(t)dt,∫−∞0f(t′)dt′=∫0∞ f(t)dt=1ρ¯sρ¯sρ¯sρ¯ equation (4) s(,π/2)ρ¯sρs(0) ρ¯sQFI≈∑i=01Re(ρi12)2(1ρi11+1ρi22)+ (ρi11−ρi22) 2ρi11+ρi22,ρ1ij=〈φi 〈1 ρs(0) φj〉

1〉ρ0ij=〈φi 〈0 ρs(0) φj〉 0〉 0〉 1〉H1=γB0·Sˆ1 Re(ρi12)ρi12ρs(0)ρ¯s S〉=12(〉 − 01〉)30%ρs(0)ρ¯s=H⊗m 0〉⊗m=H⊗H⊗···⊗H 00···0=12(0+ 1)⊗12(0+ 1)⊗···⊗12(0+)=12m(00···0〉+ 00···1〉)+···+(11···1) equation (5). In this article we generated the RoccustyrnaTM small molecule (Figures1a,1b,4,5a,5b, 5c,5d,6a,6b,6c,6d,6e) with the Geometrical Descriptors of the: Dreiding energy = 305,20 kcal/mol, MMFF94 energy = 35,06 kcal/mol, Minimal projection area = 66,49, Maximal projection area = 123,65 Minimal projection radius = 5,71 Maximal projection radius = 9,24 Length perpendicular to the max area = 1,29 Length perpendicular to the min area = 19,04 van der Waals volume = 409,41 Donor count = 5 Donor sites = 6 Acceptor count = 11 Acceptor sites = 14.

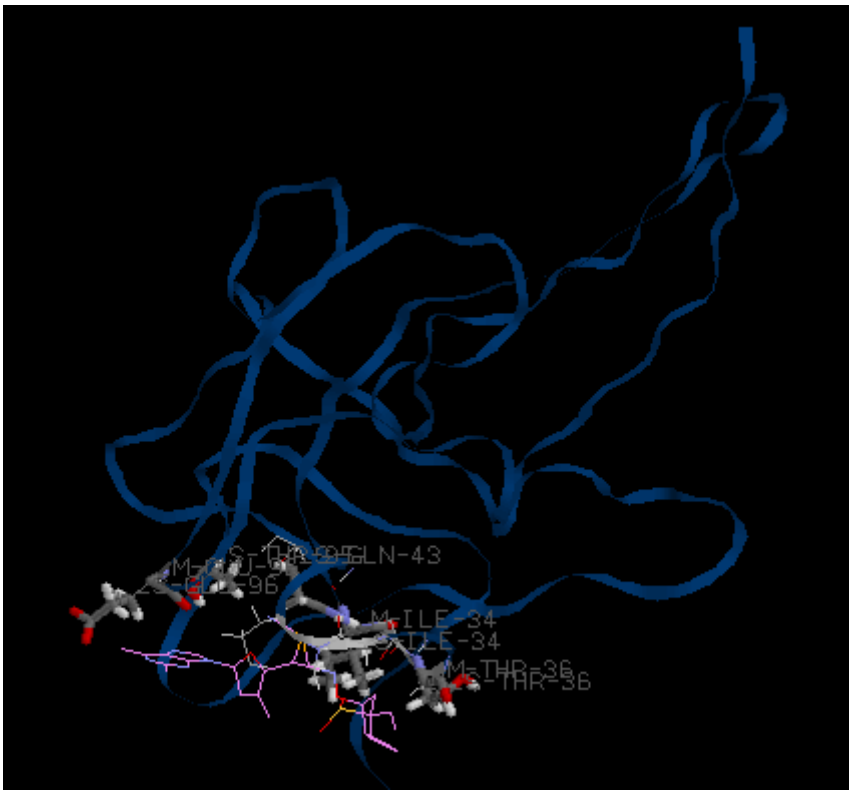

Figure8. 3D Docking interactions of the Roccustyrna small molecule (1S,2R,3S)−2−({[(1S,2S,4S,5R)−4−ethenyl−4− sulfonylbicyclo[3.2.0]heptan−2−yl]oxy}amino)−3−[(2R,5R)−5−(2−methyl−6−methylidene−6,9−dihydro−3H−purin−9−yl)−3−methylideneoxolan−2−yl]phosphirane−1−carbonitrile within the binding domains of the protein targets (PDB: 6YI3) of the N-terminal RNA-binding domain of the SARS-CoV-2 nucleocapsid phosphoprotein. The Roccustyrna ligand binds into the binding sites of the amino acids of the V-M-ILE-34, V-S-ILE-34, V-M-THR-36, V-S-THR-36, V-S-GLN-43, V-S-THR-95, V-M-GLU-96, V-S-GLU-96 with the total docking energies of the -96.6 Kcal/mol and the docking values of the -4.76839, -9.02476, -9.66643, -6.43937, -8.09017, -13.9373, -9.26627, -7.55529 Kcal/mol respectively.

(Figure7a) Electrostatic CoMFA analysis of the contact residues of the best docking poses of the contact merged chemical residues of the entire Roccustyrna chemical structure when docked onto the SARS-COV-2 protein targets, (pdb:3fqq) hits the positively charged groups and red regions favored by negatively charged groups within the binding domains sequence of the amino acid of the V-S-HIS-159, V-S-ARG-16, V-S-ARG-112, V-M-GLU-148, V-M-PHE-15, V-S-PHE-15, V-S-HIS-159, V-M-TYR-161 with the docking energy values of the -101, -14.0762, -5.11094, -7.98447, -4.17314, -4.43549, -9.66939, -9.42926, -7.30085. (Figure7b) Other QSAR/CoMFA contour map experiments of electrostatic regions of the binding interaction of

the entire pharmacophoric residues of the Roccustyrna chemical design when docked onto the SARS-COV-2 protein binding sites of the the electrostatic surface view of active site pocket of its active contact residues of the Roccustyrna small molecule when docked onto the SARS-COV-2 protein targets, (pdb:6xs6), interacted negatively with all the charged groups of the sequence of the amino acid of the V-M-LYS-557, V-S-LYS-557, V-M-ARG-567, V-M-ASP-568, V-S-ASP-574, V-S-PHE-43, V-M-ARG-44, V-M-SER-45, V-S-SER-45 with the docking energy values of the -85.8, and -5.56004, -5.0011, -8.38956, -5.77168, -6.13664, -12.8661, -5.37546, -6.10391, -5.00928 Kcal/mol respectively. (Figure7c) Moreover, Cluster of the QSAR/QMMM/CoMFA map analysis of electrostatic regions around the contact residues of the Roccustyrna small molecule when docked onto the SARS-COV-2 protein targets, (pdb:2ghv). (green, favored; yellow; disfavored) around the entire Roccustyrna chemical structure regions has shown that our innovative drug design generated negatively charged groups within the sequence of the amino acid of the H-M-ASN-33, H-S-ASN-33, H-S-TYR-356, H-M-ASN-424, V-M-ASN-33, V-M-ALA-331, V-M-THR-332, V-S-THR-332, V-S-TYR-356, V-S-TRP-423, V-S-ILE-428, V-S-ARG-495 with the docking energy values of the -104.7 and-3.45708, -3.5, -3.97711, -3.5, -5.33228, -6.79753, -7.9376, -6.69969, -12.2528, -7.66989, -8.15072, -7.00332Kcal/mol respectively. (Figure7d) In addition, CoMFA contour map of electrostatic regions around Roccustyrna chemical structure indicated that the contact residues of the Roccustyrna small molecule when docked onto the SARS-COV-2 protein targets, (pdb:2zu5). (green, favored; yellow; disfavored) around the Roccustyrna chemical structure hits the entire sequence of the amino acid of the V-M-THR-25, V-S-THR-25, V-M-THR-26, V-S-HIS-41, V-M-LEU-141, V-M-ASN-142, V-S-ASN-142, V-M-GLY-143, V-S-CYS-145, V-M-MET-165 with the binding energy values of the -97.2 and -5.16512, -4.15949, -9.8487, -4.77062, -4.72901, -6.7295, -5.82428, -5.35883, -4.2588, -5.37491 Kcal/mol respectively. (Figure7e) The Roccustyrna small molecule hits also the entire binding domains of the SARS-COV-2 protein targets, (pdb:6w9c) within the sequence of the amino acid of the V-S-PRO-59,V-S-ARG-65, V-M-THR-75, V-S-THR-75, V-M-PRO-77, V-S-PRO-77, V-M-HIS-47, V-S-HIS-47 with the docking energies of the -83.9, -4.21999, -12.6164, -7.60372, -6.69528, -5.89416, -6.40663, -5.51621, -7.99273. (Figure8) More specifically, the Roccustyrna small molecule generated also negative docking energy values with a potential inhibitory effect when docked against the sequence of the amino acids of the protein targets (PDB: 6YI3) of the N-terminal RNA-binding domain of the SARS-CoV-2 nucleocapsid phosphoprotein which is essential for linking the viral genome to the viral membrane. Finally, the Roccustyrna chemical structure generated an inhibitory docking effect of high negative binding energy docking values of the -66,7 Kcal/mol when docked onto the cav7bv2_POP binding domains within the amino acids of the V-M-LYS-551, V-S-LYS-551, V-S-ARG-553, V-S-ASP-618, V-M-TYR-619, V-M-PRO-620 with the docking energy values of the -4.71516, -10.4842, -4.7999, -6.65538, -5.1339, -6.28532Kcal/mol. On the other hand the Remdesivir drug when combined to the Roccustyrna small molecule interacted at the same binding domains of the amino acids of the V-M-LYS-551, V-S-LYS-551, V-S-ARG-553, V-S-ASP-618, V-M-TYR-619, V-M-PRO-620 with positive and zero docking values of the +42.1, -0.104885, -0.19986, +25.0575, Kcal/mol. That means that the Remdesivir drug could induce the COVID19 disease.

Discussions

In this article, we propose an alternative topological quantum computing optimization framework for the computation of topological invariants of knots, links and tangles through a discrete stochastic optimization procedure that uses nonlinear finite element analysis and a ground structure approach, as applied to quantum homology inspired Chern-Simons topology evolutionary scalable and fast fragmentation algorithm in which the geometric concepts of proper time enter in the non-relativistic limit(20-38,39). The focus of this work is to develop a Quantum Heuristic Fragmentation driven Chern-Simons fragmentation algorithm that is as independent to allow for a faster development as possible from the chosen pharmacophoric fragmentation scheme of new group contribution drug design methods. (32,35-38,40)For this reason, the Roccustyrna mutli- targeting pharmacophoric element for each pattern was kept as simple as possible and can be geometrically represented as promising potent and selective anti-viral inhibitor with rationally calculated logical atomic spaces and subatomic subspaces allowing a vectorial negative docking energy representation against this drug target. (20,25,26-39,40,41)The few chemical space patterns in this project orthogonically applied for the design of a novel multi-chemo-structure the Roccustyrna small molecule against the crystal structure of COVID-19 main protease in a Lindenbaum-Tarski generated generated QSAR automating modeling lead compound design approach. In this hybrid drug designing approach, we have designed the RoccustyrnaTM nano-structures as a system of intrinsically positioned cables filtered before evaluation and triangular bars kinematically stable and structurally valid symmetric formations of connected components, holes, and voids jointed at their ends by hinged connections to form a rigid chemical scaffold in persistent homology (19,21,24-38,40,41,42).

Conclusions

Here, for the first time we have generated drug repositioning In-Silico approaches against the COVID-19, not only for constructing, remerging and generating chemical and phytical small molecule libraries available through publically available web servers, but also for the implementation of fragmentation and recoring in-silico quantum phase experiments introducing new fragment based machine-learning virtual screening experiments and employing in-house ligand libraries applied for the design of a quantum thinking novel multi-chemo-structure against the protein targets of COVID-19 main protease, the RoccustyrnaTM small molecule. By applying the Biogenetoligandorol algorithm, a Gravitational Topological (UFs) based Quantum-Parallel Particle Swarm Inspired framework was deployed by using 2D chemical features in which a generalized procedure of Quantization of classical heuristic fields was be fused together with QSAR automating modeling. I finally developed and implemented for the two algorithms using natural Euclidean Geometric Topologies and Artificial Intelligence-Driven Predictive Neural Networks, showing that it is possible to well-defined surjective atom mapping and to automate phase group and ligand-based fragmentations based on computed diagonal chemical descriptors. By identifying chemical patterns I made use of partial small fragment derivatives with the additional MM-PBSA-WSAS binding free energy calculation difficulties that the drug designs we deal with are not orthogonal. (30-42) Both Chern-Simons theories and knot theory algorithms applied in this project into merged pharmacophoric groups. Furthermore, the geometric topology driven heuristic algorithms which were used in this project are capable of fragmenting and remerging small molecules that could not be fragmented by the algorithm of the any of the known reference databases. (2,5-42) We have illustrated the power of such an approach interpreted as distinct quantum circuit, qubit preparations, and certain 1- and 2-qudit gates in a meaningful

application to components, such as qubits. Our Biogenetoligandorol platform also offers utility to researchers simply wishing to interrogate and organize generalized Hadamard where H ← [1 1; 1 − 1]/2; (−1)(i, j)|j (2) and control-Z gates data, to create an inventory of available numerical docking ∈{0,1,000,111}and b ∈{++++,−}(3) data with particular clinical or genomic features, of the shaded tangle into two-dimensional m ×m matrix I2 ←E(m); m2-dimensional vector |Φ⟩ ←I2 →; (*maximally matrix M1 ←I2 −M0; (equation6) entangled state*) (*m-dimensional identity*) space such as available datasets or patients with particular mutations and calculate the fusion of the Roccustyrna's active fragments as it can be applied which may be used to draw independently of its drug identification quantum S ←X ⊗|0⟩ ⟨0| + C ⊗|1 W ←S(I ⊗H)M1; equation (7) capabilities. (26,29-42) More specifically, in this project we implemented Inverse Docking Algorithms with nonlinear electrodynamics indicated to us that the RoccustyrnaTM small molecules generated the highest negative docking energies as compared to other FDA approved drugs against the SARS-COV-2 viruses protein targets and while it is probably true that the injudicious use involving the management of these ideas or points can cause problems, it is also true that they do and should play an important role quantum mechanically in this drug discovery field.

Significant Statements

In this project we implemented Inverse Docking Algorithms with nonlinear electrodynamics for the designing of the RoccustyrnaTM small molecule that exerts the highest negative docking energies as compared to other FDA approved drugs when docked onto the SARS-COV-2 viruses protein targets by solving the Chern-Simons Topology Euclidean Geometric in a Lindenbaum-Tarski equations (1-7) generated QSAR automating modeling and Artificial Intelligence-Driven Predictive Neural Networks.

Acknowledgments

I would like to cordially express my special thanks of gratitude to my father and teacher (George Grigoriadis Pharmacist) as well as our principal (Nikolaos Grigoriadis Phd Pharmacist) who gave me the opportunity to generalized Hadamard gates, to apply Chern-Simons Topology Geometrics, and to do this wonderful project on the Drug Discovery and Quantum Chemistry topic, for the generation of the RoccustyrnaTM molecule, a ligand targeting COVID-19-SARS-COV-2 SPIKE D614G binding sites.

References

1. Hui DS. Epidemic and Emerging Coronaviruses (Severe Acute Respiratory Syndrome and Middle East Respiratory Syndrome). Clin Chest Med. 2017;38(1):71-86.

2. Zhu N, Zhang D, Wang W, Li X, Yang B, Song J, Novel Coronavirus from Patients with Pneumonia in China, 2019. N Engl J Med. 2020;382(8):727-33.

3. Paraskevis D, Kostaki EG, Magiorkinis G, Panayiotakopoulos G, Sourvinos G, Tsiodras S. Full-genome evolutionary analysis of the novel coronavirus (2019-nCoV) rejects the hypothesis of emergence as a result of a recent recombination event. Infect Genet Evol. 2020;79:104212.

4. Lu R, Zhao X, Li J, Niu P, Yang B, Wu H, Genomic characterisation and epidemiology of 2019 novel coronavirus: implications for virus origins and receptor binding. Lancet. 2020;395(10224):565-74.

5. Luk HKH, Li X, Fung J, Lau SKP, Woo PCY. Molecular epidemiology, evolution and phylogeny of SARS coronavirus. Infect Genet Evol. 2019;71:21-30.

6. Ziebuhr J. Molecular biology of severe acute respiratory syndrome coronavirus. Curr Opin Microbiol. 2004;7(4):412-9.

7. Weiss SR, Leibowitz JL. Coronavirus pathogenesis. Adv Virus Res. 2011;81:85-164.

8. Brian DA, Baric RS. Coronavirus genome structure and replication. Curr Top Microbiol Immunol.2005;287:1-30.

9. Narayanan K, Huang C, Makino S. SARS coronavirus accessory proteins. Virus Res.2008;133(1):113-21.

10. Arndt AL, Larson BJ, Hogue BG. A conserved domain in the coronavirus membrane protein tail is important for virus assembly. J Virol. 2010;84(21):11418-28.

11. Neuman BW, Kiss G, Kunding AH, Bhella D, Baksh MF, Connelly S, et al. A structural analysis of M protein in coronavirus assembly and morphology. J Struct Biol. 2011;174(1):11-22.

12. Siu KL, Chan CP, Kok KH, Chiu-Yat Woo P, Jin DY. Suppression of innate antiviral response by severe acute respiratory syndrome coronavirus M protein is mediated through the first transmembrane domain. Cell Mol Immunol. 2014;11(2):141-9.

13. Schoeman D, Fielding BC. Coronavirus envelope protein: current knowledge. Virol J. 2019;16(1):69.

14. Al-Tawfiq JA, Al-Homoud AH, Memish ZA. Remdesivir as a possible therapeutic option for the COVID-19. Travel Med Infect Dis. 2020:101615.

15. Agostini ML, Andres EL, Sims AC, Graham RL, Sheahan TP, Lu X, et al. Coronavirus Susceptibility to the Antiviral Remdesivir (GS-5734) Is Mediated by the Viral Polymerase and the Proofreading Exoribonuclease. mBio. 2018;9(2).

16. de Wit E, Feldmann F, Cronin J, Jordan R, Okumura A, Thomas T, et al. Prophylactic and therapeutic remdesivir (GS-5734) treatment in the rhesus macaque model of MERS-CoV infection. Proc Natl Acad Sci U S A. 2020.

17. Pilon AC, Valli M, Dametto AC, et al. NuBBEDB: an updated database to uncover chemical and biological information from Brazilian biodiversity. Sci Rep. 2017;7(1):7215. Published 2017 Aug 3. doi:10.1038/s41598-017-07451-x

18. Khot WY, Nadkar MY. The 2019 Novel Coronavirus Outbreak - A Global Threat. J Assoc Physicians India. 2020;68(3):67-71.

19. Zeng YM, Xu XL, He XQ, Tang SQ, Li Y, Huang YQ, et al. Comparative effectiveness and safety of ribavirin plus interferon-alpha, lopinavir/ritonavir plus interferon-

alpha and ribavirin plus lopinavir/ritonavir plus interferon-alphain in patients with mild to moderate novel coronavirus pneumonia. Chin Med J (Engl). 2020.

20. McGraw PN, Menzinger M, Muñuzuri AP. Harmonic resonant excitation of flow-distributed oscillation waves and Turing patterns driven at a growing boundary. Phys Rev E Stat Nonlin Soft Matter Phys. 2009 Aug;80(2 Pt 2):026209. doi: 10.1103/PhysRevE.80.026209. Epub 2009 Aug 20. PMID: 19792233.

21. Martinez MA. Compounds with therapeutic potential against novel respiratory 2019 coronavirus. Antimicrob Agents Chemother. 2020.

22. Gordon CJ, Tchesnokov EP, Feng JY, Porter DP, Gotte M. The antiviral compound remdesivir potently inhibits RNA-dependent RNA polymerase from Middle East respiratory syndrome coronavirus. J Biol Chem. 2020.

23. Sheahan TP, Sims AC, Leist SR, Schafer A, Won J, Brown AJ, et al. Comparative therapeutic efficacy of remdesivir and combination lopinavir, ritonavir, and interferon beta against MERS-CoV. Nat Commun. 2020;11(1):222.

24. Trott O, Olson AJ. AutoDock Vina: improving the speed and accuracy of docking with a new scoring function, efficient optimization, and multithreading. J Comput Chem. 2010;31(2):455-61.

25. Van Meter R, Satoh T, Ladd TD, Munro WJ, Nemoto K (2013) Path selection for quantum repeater networks. Networking Science 3(1-4): 82-95.

26. Lloyd S, Mohseni M, Rebentrost P (2014) Quantum principal component analysis. Nature Physics. 10: 631.

27. Henriques AG. What Chern-Simons theory assigns to a point. Proc Natl Acad Sci U S A. 2017 Dec 19;114(51):13418-13423. doi: 10.1073/pnas.1711591114. Epub 2017 Dec 5. PMID: 29208715; PMCID: PMC5754777.

28. Honda M. Supersymmetric Solutions and Borel Singularities for N=2 Supersymmetric Chern-Simons Theories. Phys Rev Lett. 2018 Jul 13;121(2):021601. doi: 10.1103/PhysRevLett.121.021601. PMID: 30085688.

29. Simón J. Brane Effective Actions, Kappa-Symmetry and Applications. Living Rev Relativ. 2012;15(1):3. doi: 10.12942/lrr-2012-3. Epub 2012 Feb 27. PMID: 28179834; PMCID: PMC5256004.

30. Cavaglià A, Fioravanti D, Gromov N, Tateo R. Quantum spectral curve of the N=6 supersymmetric Chern-Simons theory. Phys Rev Lett. 2014 Jul 11;113(2):021601. doi: 10.1103/PhysRevLett.113.021601. Epub 2014 Jul 11. PMID: 25062163.

31. Mabkhot YN, Alatibi F, El-Sayed NN, Al-Showiman S, Kheder NA, Wadood A, Rauf A, Bawazeer S, Hadda TB. Antimicrobial Activity of Some Novel Armed Thiophene Derivatives and Petra/Osiris/Molinspiration (POM) Analyses. Molecules. 2016 Feb 17;21(2):222. doi: 10.3390/molecules21020222. PMID: 26901173; PMCID: PMC6273311.

32. Khan T, Lawrence AJ, Azad I, Raza S, Joshi S, Khan AR. Computational Drug Designing and Prediction Of Important Parameters Using in silico Methods- A Review. Curr

Comput Aided Drug Des. 2019;15(5):384-397. doi: 10.2174/1573399815666190326120006. PMID: 30914032.

33. Ulrich, H. & Pillat, M. M. CD147 as a Target for COVID-19 Treatment: Suggested Effects of Azithromycin and Stem Cell Engagement. Stem Cell Rev. Rep. 16, 434–440 (2020).

34. Chan, J. F.-W. et al. Genomic characterization of the 2019 novel human-pathogenic coronavirus isolated from a patient with atypical pneumonia after visiting Wuhan. Emerg. Microbes Infect. 9, 221–236 (2020).

35. Kong, R. et al. COVID-19 Docking Server: A meta server for docking small molecules, peptides and antibodies against potential targets of COVID-19. Bioinformatics (2020) doi:10.1093/bioinformatics/btaa645.

36. Shi, Y. et al. D3Targets-2019-nCoV: a webserver for predicting drug targets and for multi-target and multi-site based virtual screening against COVID-19. Acta Pharm. Sin. B 1, 1239–1248 (2020).

37. de Magalhães, C. S., Almeida, D. M., Barbosa, H. J. C. & Dardenne, L. E. A dynamic niching genetic algorithm strategy for docking highly □exible ligands. Inf. Sci. 289, 206–224 (2014).

38. Van Loock P (2006) Hybrid quantum repeater using bright coherent light. Phys Rev Lett 96: 240501.

39. Zhao B, Chen ZB, Chen YA, Schmiedmayer J, Pan JW (2007) Robust creation of entanglement between remote memory qubits. Phys Rev Lett 98: 240502.

40. dos Santos, K. B., Guedes, I. A., Karl, A. L. M. & Dardenne, L. Highly Flexible Ligand Docking: Benchmarking of the DockThor Program on the LEADS-PEP Protein-peptide Dataset. J. Chem. Inf. Model. acs.jcim.9b00905 (2020)doi:10.1021/acs.jcim.9b00905.

41. O. Kadioglu, M. Saeed, H. Johannes Greten, and T. Efferth, “Identification of novel compounds against three targets of SARS CoV-2 coronavirus by combined virtual screening and supervised machine learning,” Bulletin of the World Health Organization, 202, In press.

42. Müller S. Flexible heuristic algorithm for automatic molecule fragmentation: application to the UNIFAC group contribution model. J Cheminform. 2019;11:57. Published 2019 Aug 20. doi:10.1186/s13321-019-0382-3